Towards an image quality criterion to optimize Digital Image Correlation. Use of an analytical model to optimize acquisition conditions

J.P. Goulmy[1], S. Jégou[1], L. Barrallier[1]

[1] Arts et Metiers, Institute of Technology, MSMP, HESAM Université, F-13617 Aix-en-Provence, France

Corresponding author: jean-patrick.goulmy@ensam.eu (J.P. Goulmy)

(+33) 4 42 93 82 23

Abstract

Digital image correlation (DIC) is expanding in many fields. In particular, it requires that the acquisition conditions and speckle be adapted to each application. A new methodology allowing to define the quality of the images in a fast and precise way is proposed. An analytical model based on mean intensity gradient of speckle pattern criterion and the standard deviation of displacement on images has been proposed. The model can be used on the whole image or by creating subsets in the image. Standard deviation maps of displacement are obtained. The methodology makes it possible to save a considerable amount of time compared to the full DIC calculation to optimize the image acquisition conditions, the speckle and the DIC parameters.

Keywords: Digital image correlation (DIC), Quality assessment criteria, Speckle pattern optimization

1. Introduction

Digital image correlation (DIC) is increasingly used in many fields of research and engineering [1]. This technique is not only used in the field of mechanics but also in other applications such as medicine [2], [3]. This technique can be used from images acquired by optical camera, scanning electron microscope or tomography for example. Still in full expansion, it allows the analysis of images in 2 or 3 dimensions [1], [4], [5]. In the future, it could be generalized in many fields of application in connection with smart manufacturing and the implementation of multi-scale models. The development of reliable and practical tools to facilitate its use is therefore essential.

It has been observed in the literature that the accuracy of the method depends on many factors: the computational parameters [6], [7], the sub-pixel registration algorithms [8], [9], the sub-pixel interpolation schemes [10]–[12], the camera resolution [13], the image noise [14], [15], the speckle quality [16], [17] ; or the test environment [18]–[20]. Also, the choice of parameters depends on the type of application and there are no specific rules to set them. The understanding of their impact on the results is therefore essential. Moreover, the ability for the user to modify them efficiently and quickly represents a major challenge to facilitate the implementation of this technique in many fields such as engineering.

In order to obtain a good accuracy of the measurements, one of the most important phases is the setting up of the image acquisition. This step consists in creating a speckle adapted to the desired resolution, and choose the acquisition parameters accordingly (lighting, exposure time in the case of an optical camera ...). Today, the most direct way to know if the correlation of digital images is going to be successful is to take two successive images under similar conditions and to correlate them together [21]. The results obtained can then be used to define whether the measurement is accurate, and has measurement artifacts or noise. This step is time consuming and tedious when it is necessary to optimize the acquisition parameters.

At the same time, many criteria are present in the literature to define the quality of the speckles but are still not well exploited by image correlation software [14], [17], [22]–[29]. Among the many criteria, the mean intensity gradient of speckle pattern (MIGSP) criterion represents a simple and efficient way to define the quality of the images [14], [22]. This criterion can therefore be used to define the optimal acquisition conditions.

The objective of this paper is to show how to use the MIGSP criterion to improve the quality of the images and define the accuracy of the measurements through many examples. Both a global and local approach is used with the same criteria.

First, the overall approach is exposed. The image processing is described and MIGSP criterion is introduced. Then, an analytical model allowing to link this criterion to the standard deviation of displacement is proposed. This model is then validated using a global and local approach. Finally, various examples of the use of the criterion are presented.

2. Principle

2. 1. Generation of test images

Virtual or experimental images were first created and named "image_00". Subsequently, it was necessary to generate an additional image to correlate two images. Several solutions were then possible. In the case of an experimental image, two images could be taken successively with or without strain applied. In the case of virtual or experimental images, a noise, characteristic of the difference between two successive images could be added. Based on previous experimental measurements, a normal law with a standard deviation of 15 greyscales, leading to the creation of the image "image_01" was applied [30], [31]. Then, "image_00" and "image_01" were compared with DIC software.

2. 1. 1. Creation of the virtual speckle

Virtual 8 bits images (256 grey values) of 1000 pixels by 1000 pixels were generated using MATLAB ver. R2016.a. The creation of the virtual speckle was done in two steps. First, an image with an average grey level of 20 was created. The grey levels were explicitly selected to vary within the image uniformly with a standard deviation of 15 greyscales. These values were selected because they were representative of some image backgrounds experimentally encountered. In a second step, the speckle was added. It was composed of circles whose average grey level varied according to the images and which had a normal distribution of the grey level around the average value with a standard deviation of 15. The number of particles and their radius were variable (see Table 1). The image "image_00" mentioned above was thus obtained. In order to scan a relatively wide spectrum of patterns, several parameters that influence the shape, density and grey level of the speckle were modified. The grey level of the particles *GLP* varied between 80 and 230 in steps of 50. The radius of the particles $R_{particles}$ varied from 2 to 20 pixels. The number of particles $N_{particles}$ was fixed between 1000 and 10000. The density of speckles (d_s) therefore depended on the particle size and their number. All the speckles tested led to densities ranging from 0.0063 to 1. In order to have images representative of reality, only images with speckle densities between 0.25 and 0.75 were retained. The size of the subset $R_{subregion}$ to perform the digital image correlation also varied from 20 to 60 pixels. The grey level of the image background was set to 20 and 60. Figure 1 shows some examples of the virtual speckles obtained. An image named "Image_3000_10_180" represents a speckle containing 3000 particles of radius 10 pixels and having an average grey level of 180.

Grey level of the image background	Grey level of the particles *GLP*	Radius of the particles (pixel) $R_{particles}$	Number of particles N_p	Subset Radius $R_{subregion}$
[20, 60]	[80, 130, 180, 230]	[2, 5, 10, 15, 20]	[1000, 3000, 5000, 7000, 9000]	[20, 30, 40, 50, 60]

Table 1. Set of variables selected for the study of the influence of speckle on image correlation.

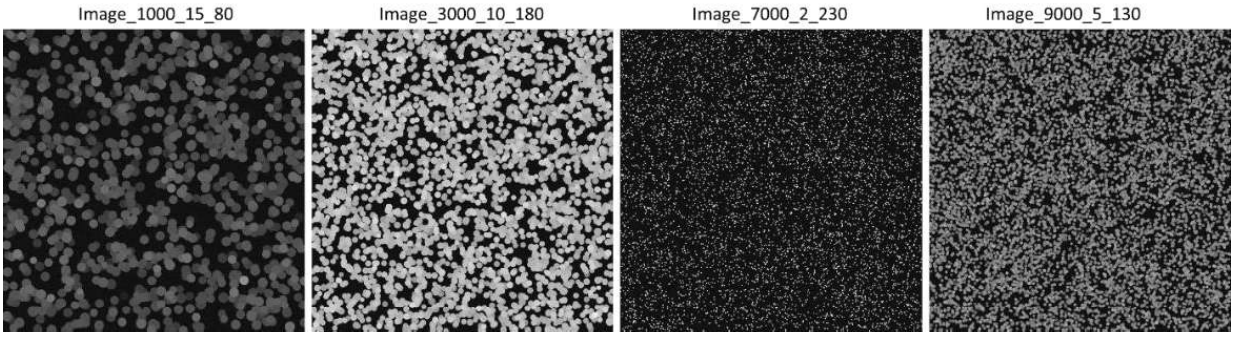

Figure 1. Examples of virtual speckles.

2. 1. 2. Creation of the experimental speckle and acquisition of the images

Three characterization techniques were used to acquire images on steel material, optical camera (OC), scanning electron microscope (SEM) and optical microscope (OM).

Optical camera (OC)

A Canon 6D Reflex camera with EF 100mm f/2.8L Macro IS USM Lens was used to acquire images. The aperture, shutter speed and ISO were dependent on the speckles and the ambient light conditions used. The resolution obtained was between 3 µm/pixel and 30 µm/pixel according to the camera lens. A classical aerosol deposition method was used to create the speckle. Alternating layers of white, black and white were deposited on the surface of the samples using paint. Numerous images obtained on different materials were characterized in this way. An example of the resulting speckle pattern is shown in Figure 2.a.

Scanning Electron Microscope (SEM)

The images were acquired using a JEOL JSM-7001F SEM. The acquisition conditions were as follows: 10 kV voltage, 9 probe current, 13 mm working distance, 4 integrated images, 5 scan speed, and secondary electrons mode. The resolution obtained was between 0.019 µm/pixel and 0.185 µm/pixel depending on the magnification used. The speckle used with OC acquisition was not adapted because the size of the particles was too large compared to the investigated resolutions. In order to carry out the acquisitions with the SEM, several speckles were dropped to the surface of steel material after mirror diamond polishing down to 1 µm followed by chemical etching using a 3% Nital solution (nitric

acid in ethanol). A drop of Al_20_3 PH 8.5 solution diluted in acetone was then deposited on the surface of the samples and dried with a hair dryer. This operation was then repeated to obtain the desired d_s. Five speckles were created for comparison. An example of the images obtained for "Speckle 1" is shown in Figure 2.b.

Optical microscope (OM)

Images were also captured using an Olympus BX41M and a UI-3280CP-C-HQ_Rev_2 camera. A resolution of 0.12 µm/pixel was used and a sample with different particle densities was observed. A typical example of the observations made is shown in Figure 2.c. The speckle deposition protocol was identical to that used to deposit the particles in the SEM images.

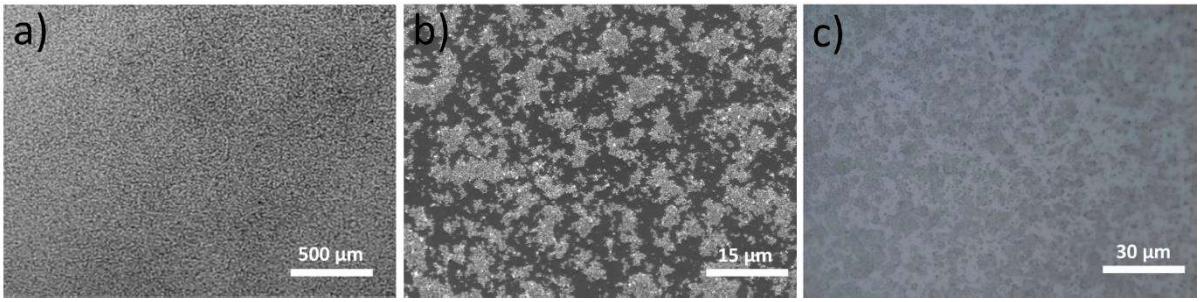

Figure 2. Examples of speckles obtained with a) the optical camera, b) the FEG JEOL JSM-7001F SEM and c) the optical microscope.

2. 2. Calculation of the displacements with the Ncorr software

The Ncorr *vers. 1.2* was used to correlate all the images [32]. Some images were also processed with DICE *vers. 2.0* [33] to compare the results with Ncorr software. The size of the analysis window φ_{window} in DIC is defined by equation (1).

$$\varphi_{window} = 2\left(R_{subregion} + P_{spacingDIC}/2 + 1\right) \quad (1)$$

Where $R_{subregion}$ represents the radius of the correlation subset, and $P_{spacingDIC}$ the pixel spacing between two measurement pixels (fixed at two here).

2. 3. Evaluation of the images quality

Two methods to evaluate the quality of the images are compared. The first method consisted in comparing "image_00" and "image_01" between them by DIC. Then, a standard deviation of displacement was calculated (equation (2)). It could be defined either from the global image or by subdividing the image by subset size equal to φ_{window}.

$$Stdu_x = \sqrt{\frac{\sum_{i=1}^{n} \left| u_{x_i} - \overline{u_x} \right|^2}{n-1}} \quad (2)$$

Where u_{xi} denotes a displacement value, $\overline{u_x}$ represents the average value of displacement and n the number of determined values.

The second method consisted in calculating, for "image_00", the value of mean intensity gradient of speckle pattern criterion named δ_f in the following [14], [22] (equation (3)).

$$\delta_f = \sum_{i=1}^{W} \sum_{j=1}^{H} \left| \nabla f(x_{ij}) \right| / (W \times H) \quad (3)$$

Where W and H represent the width and height of the image respectively. $\left| \nabla f(x_{ij}) \right| = \sqrt{f_x(x_{ij})^2 + f_y(x_{ij})^2}$ is the modulus of the local gradient vector of the intensity with $f_x(x_{ij})$ and $f_y(x_{ij})$ the derivatives in the x and y-axis directions of the image plane at the pixel (x_{ij}).

It is suggested to localize the use of the criterion δ_f by dividing the images into subsets. Thus, a local value δ_{fl}, associated with each subset of the image, could be computed (equation (4)) and represented as a mapping.

$$\delta_{fl} = \sum_{i=1}^{W_s} \sum_{j=1}^{H_s} \left| \nabla f(x_{ij}) \right| / (W_s \times H_s) \quad (4)$$

Where W_s and H_s represent the width and height of the subset.

By adjusting the subset size to the φ_{window} size used in DIC, it was then possible to predict the locations for which the speckle or the acquisition conditions were not optimal. Then, by varying the subset size, an optimal φ_{window} size allowing the highest spatial resolution without degrading the accuracy of the measurements could be identify.

3. Analytical model for defining $Stdu_x$ based on δ_f criterion

3. 1. Evolution of δ_f as a function of the standard deviation of displacement $Stdu_x$

Figure 3 shows the evolution of δ_f criterion as a function of the standard deviation of displacement $Stdu_x$. The results are similar to those obtained by Pan *et al.*, the higher the criterion, the lower the standard deviation of displacement [22]. Furthermore, the relationship between δ_f et $Stdu_x$ is independent of the type of acquisition used. These results suggest that it is possible to define an analytical model to link δ_f and $Stdu_x$.

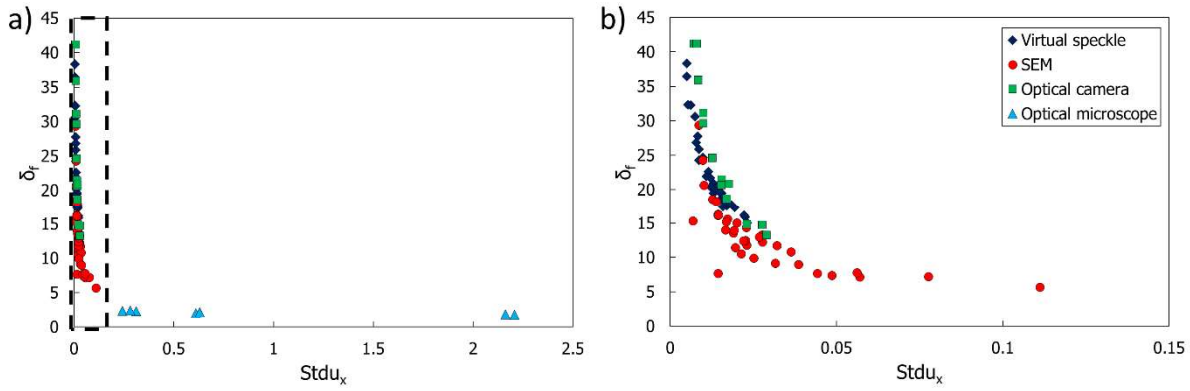

Figure 3. Evolution of δ_f as a function of the standard deviation of displacement $Stdu_x$ for different images acquisition methods. (b) is zoom of (a).

3. 2. Analytical model related to δ_f for defining image quality

Based on Figure 3, a relationship between δ_f and the standard deviation of displacement $Stdu_x$ could be defined. However, $Stdu_x$ was dependent on the analysis window size φ_{window} used by DIC software. δ_f being independent of this value, the relationship between δ_f and $Stdu_x$ was necessarily dependent on φ_{window}. In view of the observed trend between δ_f and $Stdu_x$ in log-log graph, a power law was suggested to make the link between them (equation (5)).

$$\delta_f = A_{\varphi_{window}} \, Stdu_{x\varphi_{window}}{}^{B_{\varphi_{window}}} \qquad (5)$$

Where the parameters $A_{\varphi_{window}}$ and $B_{\varphi_{window}}$ are possibly dependent on each value of φ_{window} as shown in Figure 4. The best correlation coefficient obtained between $A_{\varphi_{window}}$ and φ_{window} was obtained with a power law (equation (6)). The evolution of the parameter $B_{\varphi_{window}}$ was more difficult to reproduce. Thus, it was proposed to fix the value as a constant *B*.

$$A_{\varphi_{window}} = a\ {\varphi_{window}}^{b} \quad \textbf{(6)}$$

Where *a* and *b* were constants.

The relationship between δ_f and $Stdu_x$ was defined by a power law and is then given by equation (7):

$$\delta_f = a\ {\varphi_{window}}^{b}\ {Stdu_{x\varphi_{window}}}^{B} \quad \textbf{(7)}$$

In order to identify the parameters, only the images of virtual were selected as they gave a better accuracy. A least squares method was used to identify *a*, *b* and *B* (a = 15.56, b = -0.51 and B = -0.55). The results obtained are shown in Figure 5.

The proposed model, using δ_f and φ_{window} is a reliable method for determining the quality of the images. It can be used in two different ways. (i) Calculating δ_f on the complete image provides an estimate of the standard deviation of displacement generated by the speckle and the measurement conditions with a global approach. (ii) By subdividing the image, the value of δ_{fl} can be calculated for each subset (equation (4)) and provide more local information about the image. By inverse method, the standard deviation of displacement $Stdu_{x\varphi_{window}}$ can be calculated and displayed directly on the images.

$$Stdu_{x\varphi_{window}} = \left(\frac{\delta_{fl}}{a\ {\varphi_{window}}^{b}}\right)^{1/B} \quad \textbf{(8)}$$

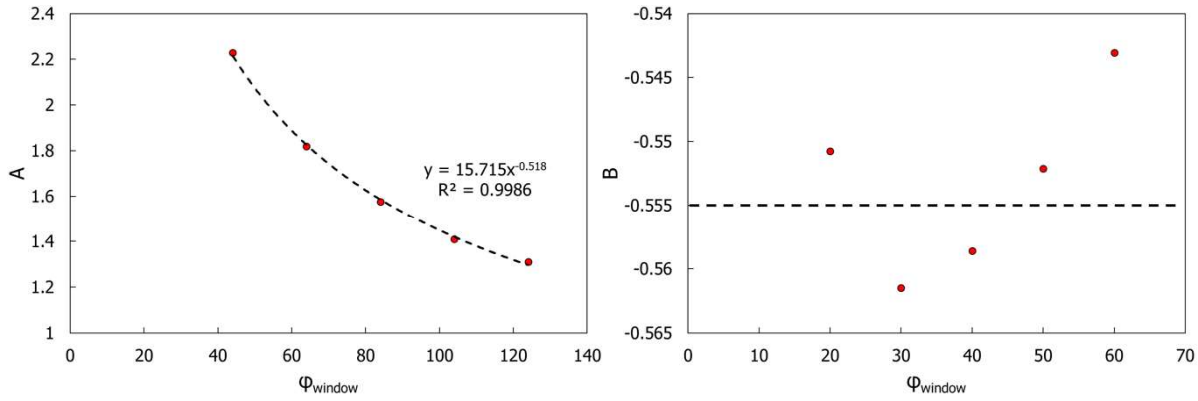

Figure 4. Evolution of the constants A and B as a function of φ_{window}.

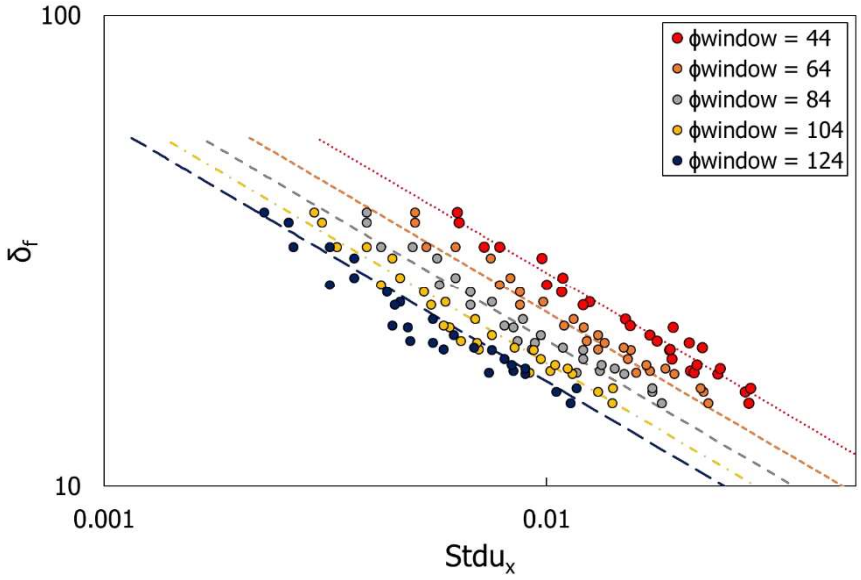

Figure 5. Evolution of the criterion δ_f as a function of the standard deviation of displacement $Stdu_x$ for different values of φ_{window}, analytical model (feature) versus Ncorr software results (symbols).

3. 3. Validation of the analytical model

Figure 6 shows the results obtained with the dataset for a window size φ_{window} = 64 pixels. Measurements made on three images with DICE software under similar calculation conditions have also been added. The model describes relatively well the evolution of δ_f as a function of the standard deviation of displacement $Stdu_x$ for a range of data from the smallest δ_f encountered to the largest and for all types of images. As previously observed, the higher the value of δ_f, the lower the gain in measurement accuracy. Therefore, it is not necessary to optimize the speckle quality or the conditions of image acquisition too much to obtain reliable image correlation values, especially when the selected

φ_{window} is large. The values calculated with the DICE correlation software follow strictly the same trend. The analytical model thus proposed is not dependent on the DIC software used, which is of great interest for its use in the future.

In addition, in order to evaluate the robustness of the methodology, repeatability measurements were performed on different images. For example, images were taken successively with an optical camera under the same acquisition conditions. Stable values of δ_f were obtained with a variation of less than 0.5%. On the other hand, when the acquisition conditions were modified, particularly notable variations of δ_f, of the order of 50%, were obtained (see section 4 .2). These results demonstrate both the stability of the criterion for the same acquisition conditions and its sensitivity when the acquisition conditions are modified.

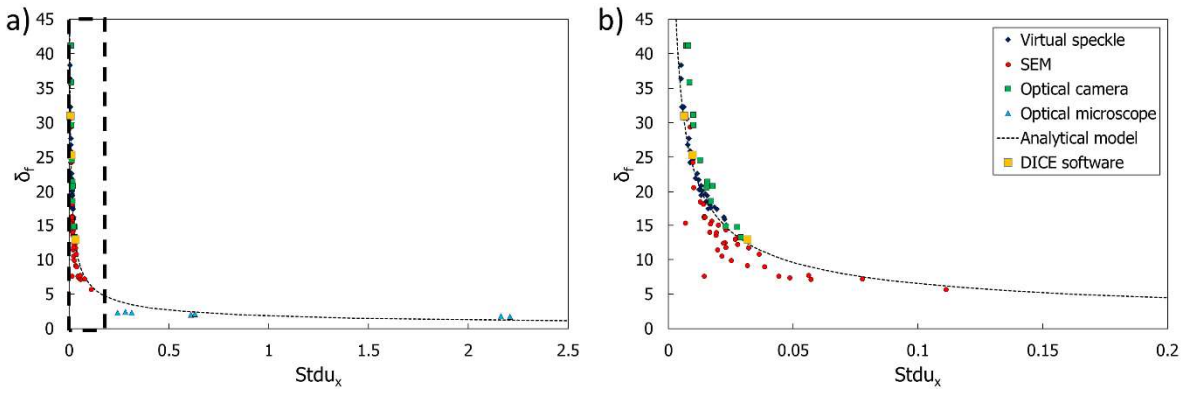

Figure 6. Validation of the model linking δ_f and $Stdu_x$ for different images acquisition methods. (b) is zoom of (a).

Figure 7 shows a comparison of standard deviation of displacement $Stdu_x$ obtained via the δ_{fl} criterion and DIC for an image captured by optical camera. Several subset sizes were used to perform the calculations. The maps obtained are very similar in terms of the distribution and in absolute $Stdu_x$ values. A gradient of values, characteristic of an inhomogeneity of the speckle or lighting conditions, is obtained for the lowest φ_{window} values. Another example to validate the proposed local approach is shown in Figure 8. The maps obtained with the two methodologies for an image acquired by SEM are very close, especially in the most critical areas.

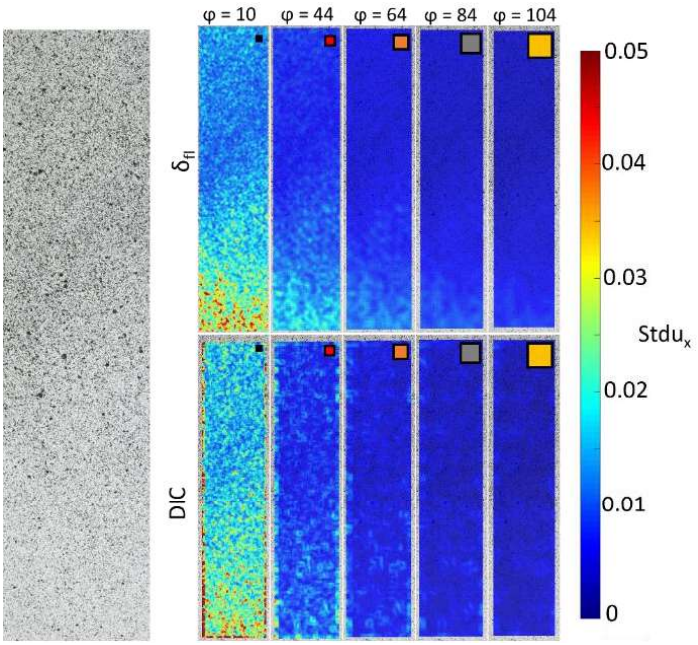

Figure 7. Comparison of standard deviation of displacement obtained via the δ_{fl} criterion and DIC for an image acquired by optical camera. The subset size used is given on top left right-hand corner.

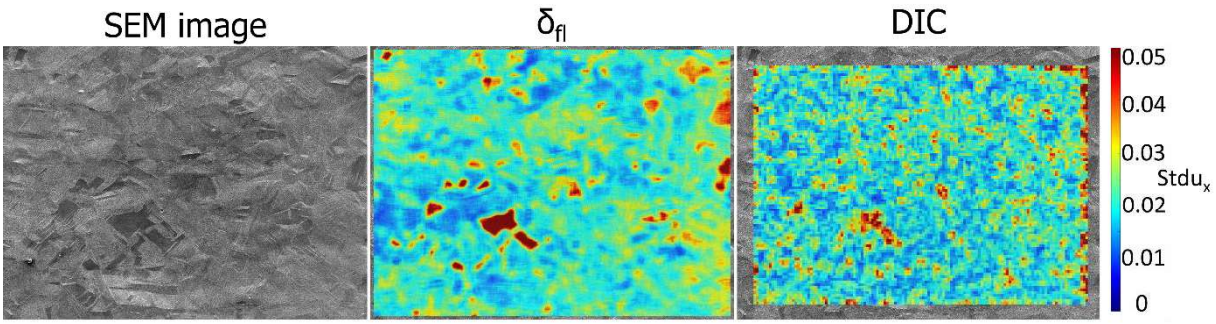

Figure 8. Comparison of standard deviation of displacement obtained via the δ_{fl} criterion and DIC for an image acquired by optical camera.

In order to represent the data in the form of a map, it is necessary to perform the calculation pixel by pixel. For images with a large number of pixels, the calculation can appear almost as long as the image correlation. However, depending on the desired accuracy, it is possible to perform the calculation only on certain pixels spaced by a value $P_{spacing\delta f}$. The set of pixels located around the calculated pixel are then defined as equal to the latter. $P_{spacing\delta f}$ is different from that used in DIC $P_{spacingDIC}$ (equation (1)). It is only used here to reduce the calculation time by reasonably degrading the mapping, it has no influence on the calculated values $Stdu_x$.

Figure 6 shows the results obtained on an image characterized by a strong standard deviation gradient of displacement for different values of $P_{spacing\delta f}$. The time associated with each calculation is present in the figure. It is obvious that using a $P_{spacing\delta f}$ less than 10 does not alter the results significantly. An optimization of the acquisition parameters is always possible under these conditions. The computation times are much smaller as soon as the spacing between the computational pixels is increased. The gain in computation time compared to DIC is then of great interest (> 10). In the following, all results are presented with $P_{spacing\delta f}$ = 1.

The methodology implemented is therefore validated and can be used to define the quality of image acquisition conditions on any type of image and at different locations in the image.

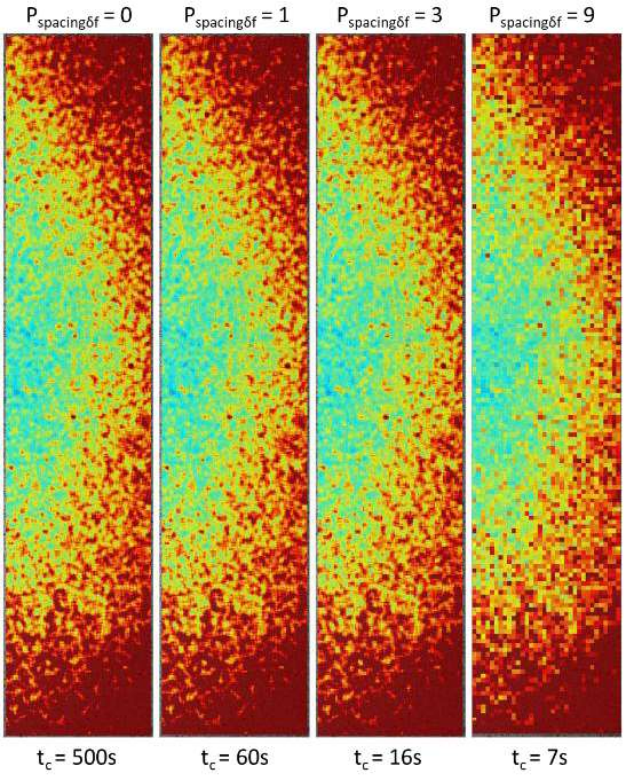

Figure 9. Comparison of mappings and computation times according to the value of $P_{spacing\delta f}$, photo 3 of Table 3, 650x3050 pixels, , φ_{window} = 24.

4. Case of studies

4. 1. Validation of speckle for multiscale approach measurements

In order to identify mechanisms (mechanical, physical, thermal ...) at different scales, it is sometimes necessary to adopt different points of view to perform the measurements. This first application case aims to show how the proposed methodology can be used to identify which type of speckle is desirable in the case of mechanical tests performed at different SEM resolutions.

4. 1. 1. Case with a deposited speckle

The material studied was 33CrMoV12-9 steel. Five speckles were deposited on the surface sample according to the protocol described below. Mirror polishing was carried out down to ¼ µm. In some cases, a chemical etching was carried out using a 3% Nital solution (nitric acid in ethanol) before applying the speckle. Then, a drop of Al_20_3 PH 8.5 solution diluted in acetone was deposited on the surface of the samples and dried with a hair dryer. This operation was then repeated (number of coating cycles) to obtain different density of particles. Five speckles were created for comparison (Table 2).

Table 2. Summary of sample preparation.

speckle number	Chemical etching	Number of coating cycles	Density of particles
1	-	25	0.47
2	Nital 3%	10	0.16
3	Nital 3%	5	0.13
4	Nital 3%	10	0.27
5	Nital 3%	10	0.28

The images were acquired at three different resolutions of 189 nm/pixel, 63 nm/pixel and 19 nm/pixel respectively. The images taken being 1280 pixels x 960 pixels, the fields of view obtained ranged from 242 µm x 181 µm to 24.2 µm x 18.1 µm.

Figure 10 shows the images acquired at different resolutions and for various speckles in SEM. For the same speckles, the densities calculated for different resolutions are close (variation of less than 5 %).

On the other hand, the distribution of the particles appears to be quite different. In the case of a resolution of 189 nm/pixel, the particles are globally distributed in a homogeneous way whereas in the case of a resolution of 19 nm/pixel, clusters of particles appear.

As expected, speckles 2 and 3 with densities below 0.25 have the lowest δ_f values. For a given speckle, an increase in resolution leads to a decrease in the criterion δ_f (Figure 11). Also, the order established between the speckles for a given resolution is similar for the other resolutions. Speckles 1 and 4 have similar values of δ_f while they do not have similar characteristics in terms of particle size, particle grey level and image contrast. This result shows once again the interest of using a global criterion to have a normalized view of the quality of the speckles.

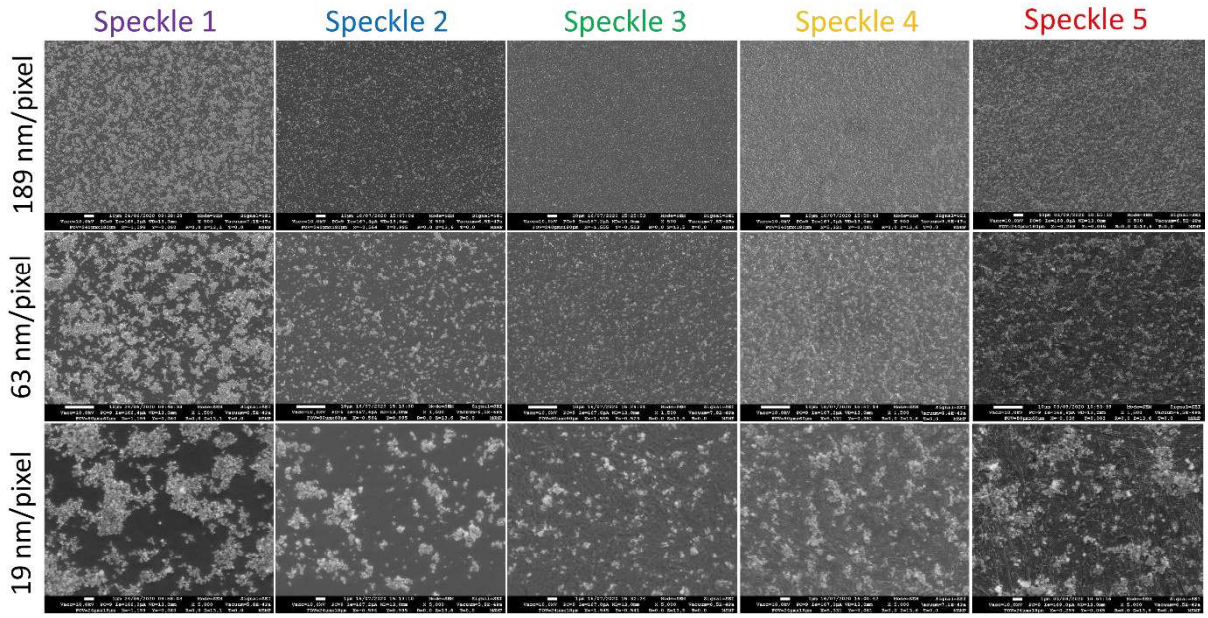

Figure 10. SEM images for different resolutions and for different applied speckles.

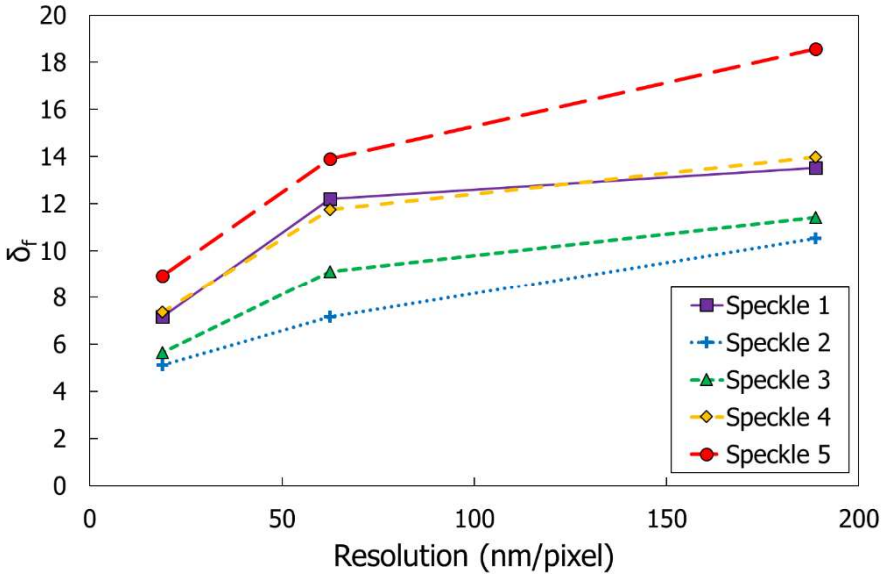

Figure 11. Evolution of δ_f as a function of resolution for different speckles.

Figure 12 shows the standard deviation maps of displacement obtained by local calculation of δ_{fl} on speckle 5, for different resolutions. These results confirm those obtained in Figure 7. The larger the resolution, the less the speckle deposited on the surface of the samples is adapted.

While one might think that large clusters of particles are detrimental to the DIC, a good correlation is obtained in these areas. In contrast, the standard deviation of displacement is greatest at the location where particles are not present. An increase in speckle density may therefore be of interest when using this kind of speckle.

Despite a higher particle density for speckle 1 conditions, the δ_f value is lower than speckle 5 conditions. Performing chemical etching before particle deposition may be of interest to generate a speckle at a different scale. The comparison of the mappings obtained at a resolution of 19 nm/pixel for speckle 1 conditions and speckle 5 conditions is particularly telling. The chemical etching performed before the deposition of speckle 5 conditions allows to deploy a secondary speckle between the clusters of particles. The standard deviation of displacement appears, certainly important in the zones without particles, but much less than for the speckle 1 conditions. Chemical etching prior to the deposition of speckles limits the areas without characteristic shapes and thus improves the correlation of the images. A better distribution of particles is also necessary to improve the quality of the DIC.

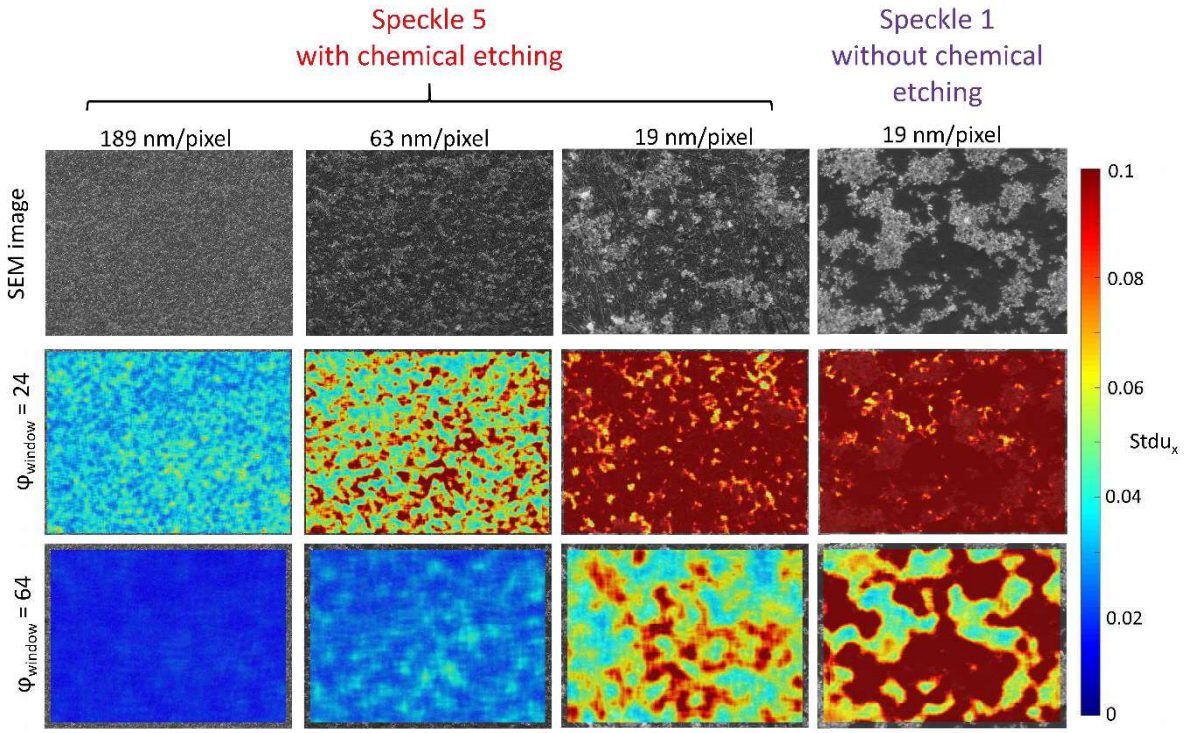

Figure 12. Standard deviation mappings of displacement obtained by local computation of δ_{fl} on speckle 5 conditions and speckle 1 conditions, for different resolutions.

4. 1. 1. Case without a deposited speckle

During multi-scale analysis, it is often interesting to couple different techniques such as Electron Back Scattered Diffraction and DIC. However, the deposition of speckles on the surface of the sample can cause a bad indexation in Electron Back Scattered Diffraction. One of the solutions is to only perform a chemical etching to reveal the natural characteristics of the samples (intragranular precipitation ...).

This exercise was performed on pure copper. A chemical etching composed of 2.5 mL $FeCl_3$ (41%), 10 mL HCl (37%) and 100 mL H_2O was used for 30 seconds to reveal the microstructure. SEM images were acquired at two different resolutions of 3.2 µm/pixel and 19 nm/pixel respectively.

The results are shown in Figure 13. The chemical etching reveals a homogeneously distributed speckle in the grains with a size around 100 nm. The grain boundaries are also clearly visible. For both investigated resolutions, the value of the standard deviation of displacement is dependent on the grey level of the grains. The darker grains induce a higher value. A complementary study showed that the

gray level of the grains was directly related to their crystallographic orientation [34]. Zooming into the grains shows that the details are less visible for the darkest grains, generating difficulties in correlation and thus a decrease in the accuracy of the measurements.

In the case where Electron Back Scattered Diffraction analysis is not desired, speckle deposition as practiced in section 4. 1. 1 could be used to improve DIC, especially for images with 3.2 µm/pixel resolution and limit correlation issues generated by grain orientation in the material.

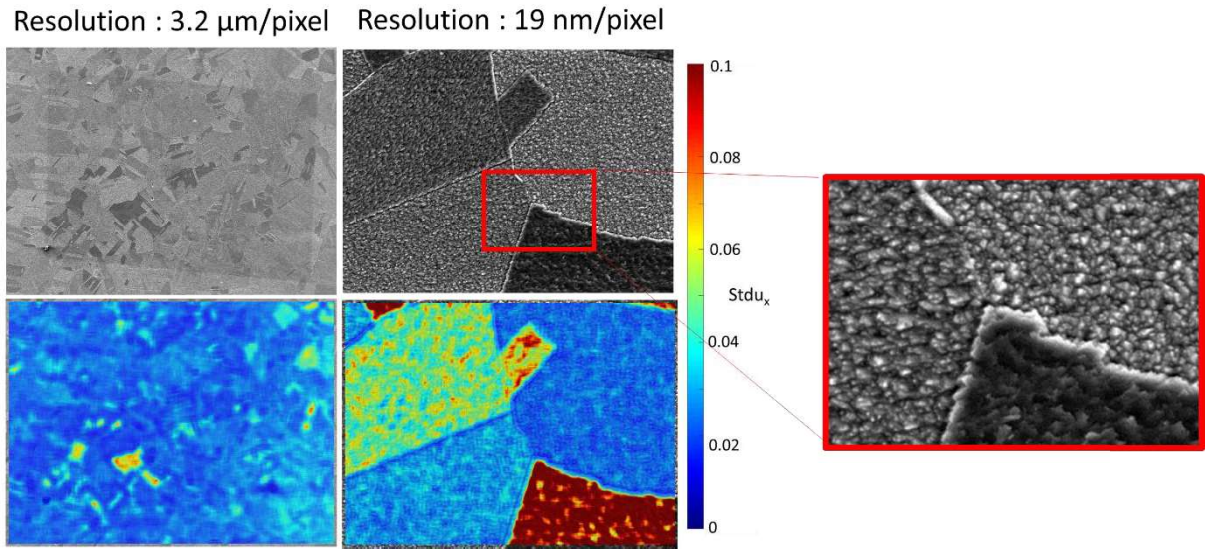

Figure 13. Standard deviation mappings of displacement obtained by local computation of δ_{fl} on pure copper after etching, φ_{window} = 24.

4. 2. Optimization of optical camera acquisition parameters

The methodology was also applied in order to identify the best possible acquisition conditions before the execution of a tensile test. The measurements were performed by Canon 6D Reflex camera with Canon EF 100mm f/2.8L Macro IS USM Lens. A speckle was deposited on a steel specimen using a black and white paint deposit as previously observed in Figure 7. The specimen was then fixed vertically with the tensile machine jaws. Thirteen images were taken with different acquisition conditions. The experimental configuration is shown in Figure 14. The parameters that were changed were: the light orientation, the light intensity, the aperture, the shutter speed and the ISO (Table 3). A high-angled

light means that the light source is facing the sample (Figure 14.b). A low-angled light means that the light source is grazing the sample (Figure 14.c).

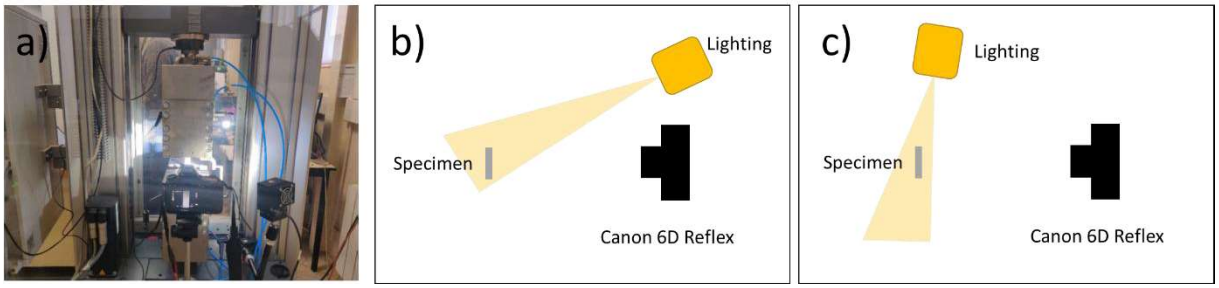

Figure 14. a) Image of the experimental setup, b) top view diagram of the High-angled light setup and c), top view diagram of the Low-angled light setup.

The results are presented in Table 3, Figure 15 and Figure 16. The values and gradients of standard deviation of displacement are more or less pronounced depending on the acquisition conditions. When the orientation of the light is close to the normal to the surface, the gradient and absolute values of the standard deviation of displacement are higher than in the grazing incidence case. It is therefore preferable to work with a grazing light.

Then, the maps are relatively similar with some small variations. For the same conditions of acquisition of the optical camera (Aperture, Shutter speed and ISO), a weak lighting is preferable to a strong lighting (images 5 and 4 respectively).

Decreasing the aperture value (images 5, 6, 7 and 8) increases the value of $Stdu_x$ by a minor amount. However, a decrease in aperture leads to an increase in depth of field which can be particularly useful in mechanical testing because of the presence of out-of-plane movements during the test. Since the impact of the aperture is small on $Stdu_x$ value, an f14 aperture is favored.

The shutter speed has a more marked impact (images 9, 10, 11 and 8). A decrease in this parameter leads to a decrease in the standard deviation of displacement. A significant difference is obtained between 1/100 and 1/160. The higher the shutter speed, the lower the amount of light captured by the camera. Between 1/100 and 1/160 the amount of light captured by the sensor is 1.6 times greater.

While between 1/160 and 1/200 the amount of light captured by the sensor is only 1.25 times greater. Thus the greatest differences are observed between 1/100 and 1/160. Another criterion can have an influence on the choice of shutter speed. In the case where the object is moving, it is necessary to adopt the lowest possible exposure time to limit the blur. The image is immobile, a high or low exposure time can be selected without major impact on the blur of the image. The only criterion that affects the choice of the parameter is the amount of light that reaches the sensor. In this case, a decrease in shutter speed leads to a better contrast of the image and therefore a higher δ_f value. The shutter speed 1/250 is therefore selected.

Finally, the ISO also plays a major role since an increase in ISO leads to an increase in the standard deviation of displacement. In the case of measurements by DIC, it is preferable to work with the lowest possible ISO to limit noise in the images. This parameter should also be taken into account when defining the acquisition conditions.

Finally, the best conditions are obtained for an aperture f11, a shutter speed 1/250 and an ISO 6400. These optimal conditions must be adapted to the ambient light, the added lighting and the nature of the speckles. By changing the amount of black or white spots on the specimen these parameters can quickly become obsolete. The use of a tool as presented in this work appears to be a quick and efficient solution to determine the best acquisition conditions for any type of configuration.

Note also that the gradient of standard deviation of displacement located at the top and bottom of the images and particularly visible depending on the conditions could be related to the reflection of light induced by the jaws holding the specimen (Figure 12). This reflection generates a local overexposure at the extreme ends of the specimen. The use of black masks on the jaws could improve the homogeneity of the image.

Table 3. Test matrix for optimization of conditions by optical camera acquisition.

Photo	Light orientation	Light intensity	Aperture	Shutter speed	ISO	δ_f	$Stdu_x$
1	High-angled light	Low	f18	1/400	2000	14.9	0.056
2	High-angled light	Low	f18	1/800	2000	13.0	0.072
3	High-angled light	High	f18	1/500	2000	14.7	0.058
4	Low-angled light	Low	f10	1/250	6400	19.5	0.035
5	Low-angled light	Low	f10	1/250	6400	23.0	0.026
6	Low-angled light	Low	f11	1/250	6400	23.0	0.026
7	Low-angled light	Low	f13	1/250	6400	22.3	0.027
8	Low-angled light	Low	f14	1/250	6400	21.3	0.029
9	Low-angled light	Low	f14	1/100	6400	18.8	0.037
10	Low-angled light	Low	f14	1/160	6400	21.0	0.030
11	Low-angled light	Low	f14	1/200	6400	21.4	0.029
12	Low-angled light	Low	f14	1/250	8000	21.4	0.029
13	Low-angled light	Low	f14	1/250	12800	19.7	0.034

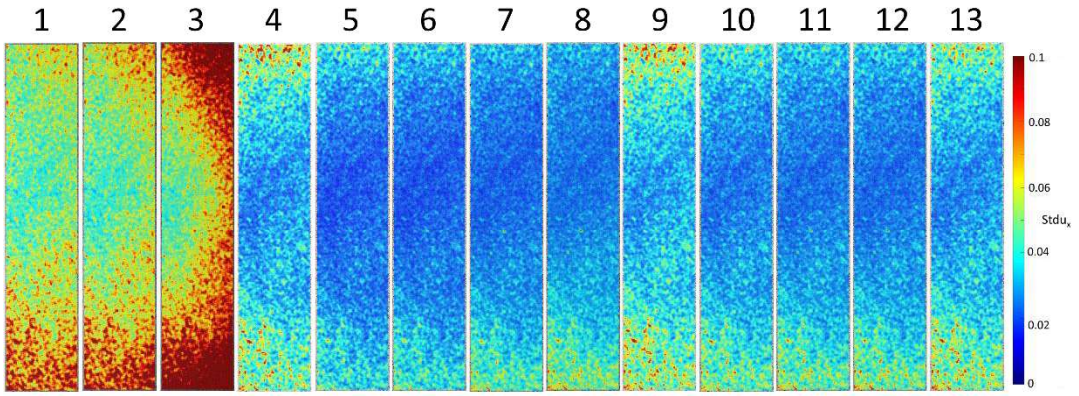

Figure 15. Standard deviation mappings of displacement obtained by local computation of δ_{fi} on images obtained by optical camera, $\varphi_{window} = 24$.

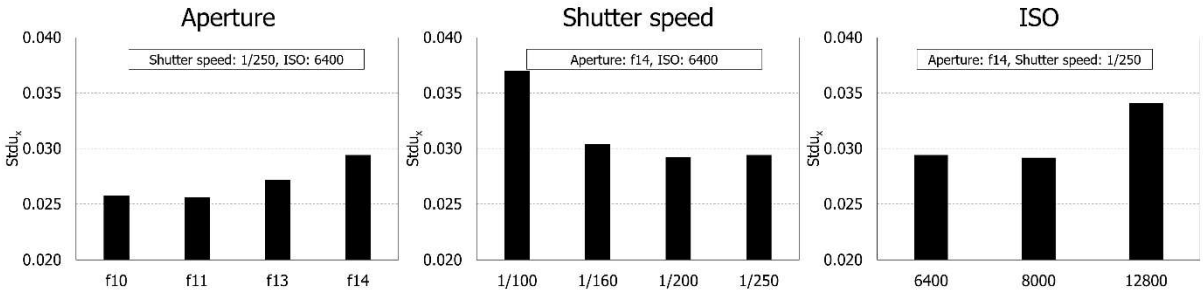

Figure 16. Evolution of the standard deviation of displacement according to the different acquisition parameters of the optical camera.

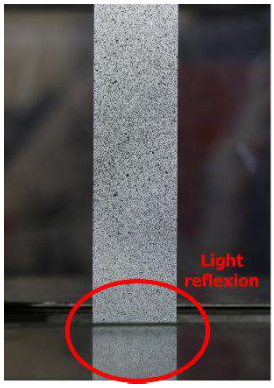

Figure 17. Optical camera picture of the steel specimen before a tensile test.

4. 3. Example of different speckles

Examples of the images and associated δ_f values are shown in Figure 18. For visualization purposes, the initial set of images was cropped to have images of 250 pixels by 250 pixels. The images obtained using the optical camera have large δ_f values. It is remarkable that a decrease in the size of the particles or clusters leads to an increase in the criterion. Some SEM images are characterized by δ_f values greater than 25 due to the presence of small silver particles that are around 50 nm in diameter. On the other hand, the absence of markers on the surface is clearly detrimental to the accuracy of the measurements when the surface does not have enough asperities by itself (SEM III image).

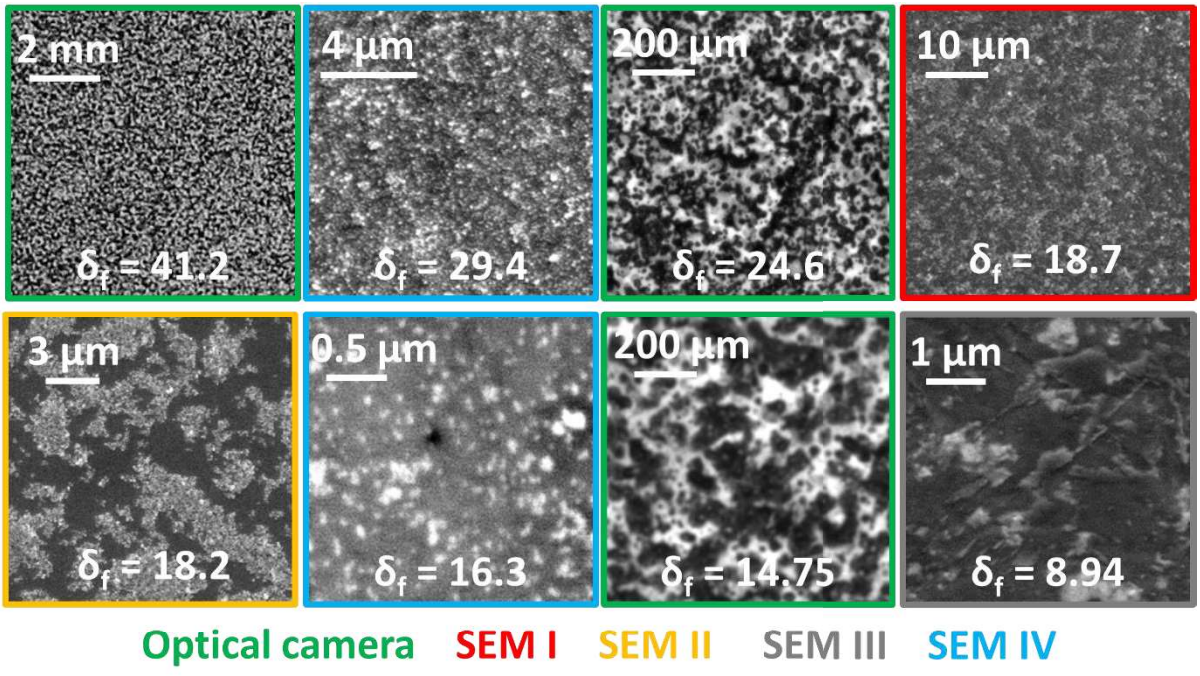

Figure 18. Examples of images and associated δ_f values, images of 250 pixels by 250 pixels.

5. Conclusion

In this paper, an analytical model linking an image quality criterion to the standard deviation of displacement computed in DIC has been proposed. The criterion, initially global, was then localized to propose standard deviation maps of displacement. These maps allow the visualization of the gradients of standard deviation of displacement.

This model was validated by comparing it to different DIC data. Also, this model does not appear to be dependent on the software used since the results obtained by DICE and Ncorr are similar. Further comparisons with different software could be performed to confirm these results.

To perform the DIC, two images are required and the computation time can be particularly long depending on the image processing conditions.

With the proposed methodology, only one image is needed and the computation time is considerably reduced. A global standard deviation of displacement value is obtained after two seconds (and this even for 5000x9000 pixels images) and a mapping with a good resolution takes less than 20 seconds to be created. At the same time, DIC under the same conditions takes longer (over 5 minutes). The time saving obtained with the proposed methodology is all the greater as the size of the images is high.

Different case studies, demonstrating the usefulness of this methodology, have been presented. The analytical model allows to determine the optimal speckle conditions but also the test conditions whatever the tool used to acquire the images. For example, it was shown that in the case of multiscale SEM analysis, the application of a chemical etching before the speckle deposition was particularly interesting to create a secondary speckle.

Acknowledgments

This research did not receive any specific grant from funding agencies in the public, commercial, or not-for-profit sectors.

References

[1] J. Zhao, Y. Sang, and F. Duan, "The state of the art of two-dimensional digital image correlation computational method," *Engineering Reports*, vol. 1, no. 2, p. e12038, 2019, doi: 10.1002/eng2.12038.

[2] T. Y.-F. Chen, P.-S. Huang, and S.-F. Chuang, "Modeling dental composite shrinkage by digital image correlation and finite element methods," *Optics and Lasers in Engineering*, vol. 61, pp. 23–30, Oct. 2014, doi: 10.1016/j.optlaseng.2014.04.006.

[3] M. Pellet, A. Chenel, M. Behr, and L. Thollon, "Is digital image correlation able to detect any mechanical effect of cranial osteopathic manipulation? – A preliminary study," *International Journal of Osteopathic Medicine*, vol. 29, pp. 10–14, Sep. 2018, doi: 10.1016/j.ijosm.2018.07.004.

[4] H. Tu, Z. Gao, C. Bai, S. Lan, Y. Wang, and Q. Zhang, "Single-camera 3D-DIC system based on a fiber bundle," *Optics and Lasers in Engineering*, vol. 147, p. 106743, Dec. 2021, doi: 10.1016/j.optlaseng.2021.106743.

[5] P. Hu, S. Yang, G. Zhang, and H. Deng, "High-speed and accurate 3D shape measurement using DIC-assisted phase matching and triple-scanning," *Optics and Lasers in Engineering*, vol. 147, p. 106725, Dec. 2021, doi: 10.1016/j.optlaseng.2021.106725.

[6] H. W. Schreier and M. A. Sutton, "Systematic errors in digital image correlation due to undermatched subset shape functions," *Experimental Mechanics*, vol. 42, no. 3, pp. 303–310, Sep. 2002, doi: 10.1007/BF02410987.

[7] X. Xu, Y. Su, Y. Cai, T. Cheng, and Q. Zhang, "Effects of Various Shape Functions and Subset Size in Local Deformation Measurements Using DIC," *Exp Mech*, vol. 55, no. 8, pp. 1575–1590, Oct. 2015, doi: 10.1007/s11340-015-0054-9.

[8] X. Shao, X. Dai, and X. He, "Noise robustness and parallel computation of the inverse compositional Gauss–Newton algorithm in digital image correlation," *Optics and Lasers in Engineering*, vol. 71, pp. 9–19, Aug. 2015, doi: 10.1016/j.optlaseng.2015.03.005.

[9] P. Bing, X. Hui-min, X. Bo-qin, and D. Fu-long, "Performance of sub-pixel registration algorithms in digital image correlation," *Meas. Sci. Technol.*, vol. 17, no. 6, pp. 1615–1621, May 2006, doi: 10.1088/0957-0233/17/6/045.

[10] H. W. Schreier, J. R. Braasch, and M. A. Sutton, "Systematic errors in digital image correlation caused by intensity interpolation," *OE*, vol. 39, no. 11, pp. 2915–2921, Nov. 2000, doi: 10.1117/1.1314593.

[11] L. Luu, Z. Wang, M. Vo, T. Hoang, and J. Ma, "Accuracy enhancement of digital image correlation with B-spline interpolation," *Opt. Lett., OL*, vol. 36, no. 16, pp. 3070–3072, Aug. 2011, doi: 10.1364/OL.36.003070.

[12] Y. Su, Q. Zhang, Z. Gao, X. Xu, and X. Wu, "Fourier-based interpolation bias prediction in digital image correlation," *Opt. Express, OE*, vol. 23, no. 15, pp. 19242–19260, Jul. 2015, doi: 10.1364/OE.23.019242.

[13] P. L. Reu, W. Sweatt, T. Miller, and D. Fleming, "Camera System Resolution and its Influence on Digital Image Correlation," *Exp Mech*, vol. 55, no. 1, pp. 9–25, Jan. 2015, doi: 10.1007/s11340-014-9886-y.

[14] Z. Y. Wang, H. Q. Li, J. W. Tong, and J. T. Ruan, "Statistical Analysis of the Effect of Intensity Pattern Noise on the Displacement Measurement Precision of Digital Image Correlation Using Self-correlated Images," *Exp Mech*, vol. 47, no. 5, pp. 701–707, Oct. 2007, doi: 10.1007/s11340-006-9005-9.

[15] Y. Wang, M. Sutton, H. Bruck, and H. Schreier, "Quantitative Error Assessment in Pattern Matching: Effects of Intensity Pattern Noise, Interpolation, Strain and Image Contrast on Motion Measurements," 2009, doi: 10.1111/J.1475-1305.2008.00592.X.

[16] D. Lecompte *et al.*, “Quality assessment of speckle patterns for digital image correlation,” *Optics and Lasers in Engineering*, vol. 44, no. 11, pp. 1132–1145, Nov. 2006, doi: 10.1016/j.optlaseng.2005.10.004.
[17] Y. Su, Q. Zhang, X. Xu, and Z. Gao, “Quality assessment of speckle patterns for DIC by consideration of both systematic errors and random errors,” *Optics and Lasers in Engineering*, vol. 86, pp. 132–142, Nov. 2016, doi: 10.1016/j.optlaseng.2016.05.019.
[18] B. M. B. Grant, H. J. Stone, P. J. Withers, and M. Preuss, “High-temperature strain field measurement using digital image correlation,” *The Journal of Strain Analysis for Engineering Design*, vol. 44, no. 4, pp. 263–271, May 2009, doi: 10.1243/03093247JSA478.
[19] S. Ma, J. Pang, and Q. Ma, “The systematic error in digital image correlation induced by self-heating of a digital camera,” *Measurement Science and Technology*, vol. 23, p. 025403, Feb. 2012, doi: 10.1088/0957-0233/23/2/025403.
[20] Y. Q. Su, X. F. Yao, S. Wang, and Y. J. Ma, “Improvement on measurement accuracy of high-temperature DIC by grayscale-average technique,” *Optics and Lasers in Engineering*, vol. 75, pp. 10–16, Dec. 2015, doi: 10.1016/j.optlaseng.2015.06.003.
[21] T. C. Chu, W. F. Ranson, and M. A. Sutton, “Applications of digital-image-correlation techniques to experimental mechanics,” *Experimental Mechanics*, vol. 25, no. 3, pp. 232–244, Sep. 1985, doi: 10.1007/BF02325092.
[22] B. Pan, Z. Lu, and H. Xie, “Mean intensity gradient: An effective global parameter for quality assessment of the speckle patterns used in digital image correlation,” *Optics and Lasers in Engineering*, vol. 48, no. 4, pp. 469–477, Apr. 2010, doi: 10.1016/j.optlaseng.2009.08.010.
[23] C. Lane, R. L. Burguete, and A. Shterenlikht, “An objective criterion for the selection of an optimum DIC pattern and subset size,” in *Proceedings of the XIth international congress and exposition*, 2008, pp. 1–9.
[24] T. Hua, H. Xie, S. Wang, Z. Hu, P. Chen, and Q. Zhang, “Evaluation of the quality of a speckle pattern in the digital image correlation method by mean subset fluctuation,” *Optics & Laser Technology*, vol. 43, no. 1, pp. 9–13, Feb. 2011, doi: 10.1016/j.optlastec.2010.04.010.
[25] H. Yu, R. Guo, H. Xia, F. Yan, Y. Zhang, and T. He, “Application of the mean intensity of the second derivative in evaluating the speckle patterns in digital image correlation,” *Optics and Lasers in Engineering*, vol. 60, pp. 32–37, Sep. 2014, doi: 10.1016/j.optlaseng.2014.03.015.
[26] J. Park, S. Yoon, T.-H. Kwon, and K. Park, “Assessment of speckle-pattern quality in digital image correlation based on gray intensity and speckle morphology,” *Optics and Lasers in Engineering*, vol. 91, pp. 62–72, Apr. 2017, doi: 10.1016/j.optlaseng.2016.11.001.
[27] G. F. Bomarito, J. D. Hochhalter, T. J. Ruggles, and A. H. Cannon, “Increasing accuracy and precision of digital image correlation through pattern optimization,” *Optics and Lasers in Engineering*, vol. 91, pp. 73–85, Apr. 2017, doi: 10.1016/j.optlaseng.2016.11.005.
[28] Y. L. Dong and B. Pan, “A Review of Speckle Pattern Fabrication and Assessment for Digital Image Correlation,” *Exp Mech*, vol. 57, no. 8, pp. 1161–1181, Oct. 2017, doi: 10.1007/s11340-017-0283-1.
[29] J. Song, J. Yang, F. Liu, and K. Lu, “Quality assessment of laser speckle patterns for digital image correlation by a Multi-Factor Fusion Index,” *Optics and Lasers in Engineering*, vol. 124, p. 105822, Jan. 2020, doi: 10.1016/j.optlaseng.2019.105822.
[30] Z. Chen, X. Shao, X. Xu, and X. He, “Optimized digital speckle patterns for digital image correlation by consideration of both accuracy and efficiency,” *Applied Optics*, vol. 57, p. 884, Feb. 2018, doi: 10.1364/AO.57.000884.
[31] M. Rossi, P. Lava, F. Pierron, D. Debruyne, and M. Sasso, “Effect of DIC Spatial Resolution, Noise and Interpolation Error on Identification Results with the VFM,” *Strain*, vol. 51, no. 3, pp. 206–222, 2015, doi: 10.1111/str.12134.
[32] J. Blaber, B. Adair, and A. Antoniou, “Ncorr: Open-Source 2D Digital Image Correlation Matlab Software,” *Exp Mech*, vol. 55, no. 6, pp. 1105–1122, Jul. 2015, doi: 10.1007/s11340-015-0009-1.
[33] D. Z. Turner, “Digital image correlation engine (DICe) reference manual,” *Sandia Report, SAND2015-10606 O*, 2015.

[34] P. J. Szabo and I. Kardos, “Correlation between grain orientation and the shade of color etching,” *Materials Characterization*, vol. 61, no. 8, pp. 814–817, Aug. 2010, doi: 10.1016/j.matchar.2010.05.005.